Published in final edited form as:
J Am Chem Soc. 2009 December 16; 131(49): 17860–17870. doi:10.1021/ja906131b.

Energetics of allosteric negative coupling in the zinc sensor *S. aureus* CzrA

Nicholas E. Grossoehme and **David P. Giedroc***
Department of Chemistry, Indiana University, Bloomington, IN 47405-7102

Abstract

The linked equilibria of an allosterically regulated protein are defined by the structures, residue-specific dynamics and global energetics of interconversion among all relevant allosteric states. Here, we use isothermal titration calorimetry (ITC) to probe the global thermodynamics of allosteric negative regulation of the binding of the paradigm ArsR-family zinc sensing repressor *Staphylococcus aureus* CzrA to the *czr* DNA operator (CzrO) by Zn^{2+}. Zn^{2+} binds to the two identical binding sites on the free CzrA homodimer in two discernable steps. A larger entropic driving force $\Delta(-T\Delta S)$ of −4.7 kcal mol^{-1} and a more negative ΔC_p characterize the binding of the first Zn^{2+} relative to the second. These features suggest a modest structural transition in forming the Zn_1 state followed by a quenching of the internal dynamics on filling the second zinc site, which collectively drive homotropic negative cooperativity of Zn^{2+} binding ($\Delta(\Delta G)$=1.8 kcal mol^{-1}). Negative homotropic cooperativity also characterizes Zn^{2+} binding to the CzrA•CzrO complex ($\Delta(\Delta G)$=1.3 kcal mol^{-1}), although the underlying energetics are vastly different, with homotropic $\Delta(\Delta H)$ and $\Delta(-T\Delta S)$ values both small and slightly positive. In short, Zn^{2+} binding to the complex fails to induce a large structural or dynamical change in the CzrA bound to the operator. The strong heterotropic negative linkage in this system (ΔG_c^t = 6.3 kcal mol^{-1}) therefore derives from the vastly different structures of the apo-CzrA and CzrA•CzrO reference states (ΔH_c^t= 9.4 kcal mol^{-1}) in a way that is reinforced by a global rigidification of the allosterically inhibited Zn_2 state off the DNA ($T\Delta S_c^t$ = −3.1 kcal mol^{-1}, *i.e.*, ΔS_c^t>0). The implications of these findings for other metalloregulatory proteins are discussed.

Introduction

The now classical theoretical models of protein allostery were developed to explain the binding of a ligand at one site on the affinity of the same or different ligand at a distant site in an oligomeric protein.[1,2] Historically, this kind of allostery is strongly rooted in changes in quaternary structure that could potentially explain both homotropic (how ligand binding influences the binding of the same ligand to subsequent sites on the oligomer) and heterotropic (how ligand binding influences the binding of a second ligand) allostery. Such structure-based allostery is further predicted to be governed by a net enthalpic component, ΔH_c, that is of the same sign as the net free energy of cooperativity, ΔG_c, be it positive allostery (ΔG_c<0) or negative allostery (ΔG>0).[3] More recent views of allostery posit that a backbone conformational change may not be necessary for communication between ligand binding sites[4] and that a change in the dynamics at a site distant from a ligand binding site(s) might make a major contribution to the allosteric response[5] (for reviews, see references[6,7]). Such an

giedroc@indiana.edu.

Supporting Information Available: Tables of raw thermodynamic data, the results of calculations of solvent accessible surface area and gel filtration analysis of Zn_2•CzrA•CzrO complexes can be found here. This material is available free of charge via the Internet at http://pubs.asc.org.

allosteric driving force originates with a change in backbone or side chain conformational entropies upon ligand binding,[8] which may result in a redistribution of populations of conformational microstates at longer timescales.[3,9] This type of allostery is predicted to occur with an overall net entropic component that is positive ($\Delta S_c>0$) for positive linkage ($\Delta G_c<0$), and negative for negative linkage. Thus, in the simplest case, three types of allosteric effects can be envisioned: Type I is governed completely by entropy (minimal, if any, backbone structural change), Type II contains entropic and enthalpic components (small structural changes accompany changes in dynamics) and Type III is entirely enthalpic in origin (a conformational change leads to a significant change in the ground-state structure of a binding site).

A metalloregulatory protein is an example of a specialized allosteric protein since binding of a metal ion triggers an allosteric response that propagates to the DNA binding interface resulting in an increased (positive regulation) or decreased (negative regulation) affinity for the operator DNA. *Staphylococcus aureus* CzrA is a paradigm member of the ArsR (or SmtB/ArsR) family of allosteric regulators[10,11] that possesses features characteristic of many classical allosteric proteins, *i.e.*, the allosteric metal ions bind to sites positioned at subunit interfaces within a homo-oligomer far from the DNA binding site; as a result, CzrA has been the subject of detailed structural and thermodynamic studies.[12–15] Like other homo-oligomeric allosteric proteins, CzrA incorporates homotropic allostery in the binding of the two Zn^{2+} ions to the homodimer that is superimposed on heterotropic allostery of Zn^{2+}-dependent regulation of DNA operator binding, the energetic basis of which is essentially unexplored.[12]

In *S. aureus*, CzrA negatively regulates the transcription of the *czrAB* operon in response to the addition of Zn^{2+} and Co^{2+} salts to the growth media.[16,17] CzrB is a cation diffusion facilitator (CDF) family efflux pump[18,19] that protects *S. aureus* from metal toxicity. CzrA binds to the operator/promoter region of *czrAB* and represses transcription; Zn^{2+} binding lowers the affinity of CzrA for the *czr* operator (denoted CzrO), leading to derepression of *czrAB*. ArsR family proteins adopt an elongated dimeric winged-helical DNA binding fold of the general architecture α1-α2-α3-αR-β1-β2-α5 with the dimer interface primarily formed by the α1 and α5 helices (Figure 1a).[12] The location of the metal sensing sites provides a further subclassification of ArsR family repressors: α5 sensors bind the regulatory metal at the dimer interface between the symmetry related C-terminal α5 helices, while α3, α3N and α4C sensors harbor regulatory sites from other helices in the molecule.[20,21] CzrA is a α5 sensor that binds Zn^{2+} or Co^{2+} in a tetrahedral coordination geometry with Asp84 and His86 from one protomer and His97′ and His100′ from the opposite protomer providing ligands to the metal ion (Figure 1a).[12]

A quantitative measure of the degree to which a ligand binding induces an allosteric response in a protein is the magnitude of the allosteric coupling free energy, ΔG_c.[11] ΔG_c^t is related to K_c^t by eq 1

$$\Delta G_c^t = -RT\ln K_c^t \quad (1)$$

which describes the overall (superscript *t*=total) ligand exchange that is consistent with the coupled equilibrium scheme shown (Figure 1b). For an allosteric activator, ligand (Zn^{2+}) binding enhances the affinity of the protein for the other ligand (CzrO in this case) resulting in $\Delta G_c < 0$ and a corresponding shift in the equilibrium to the doubly-liganded and apo states. Alternatively, an allosteric inhibitor reduces the affinity of the protein for the second ligand and $\Delta G_c > 0$, thereby shifting the equilibrium to the single-ligated states, *i.e.*, to the left (Figure 1b). This latter case characterizes CzrA since Zn^{2+} binding drives dissociation of CzrA from

the CzrO resulting in derepression of *czrAB* transcription and zinc detoxification by cytosolic efflux. ΔG_c measured from a reduction in the CzrO binding affinity of a single apo CzrA dimer relative to Zn_2 CzrA, *i.e.* the logarithmic ratio of the vertical equilibria defined by K_4 and K_3 in Figure 1b, is large and positive and on the order of ≈6 kcal mol^{-1}.[13,14]

In previous studies, we investigated the structures and residue-specific dynamics of three of the four allosteric states in this system: P, (apo-CzrA dimer), P•D (CzrA•CzrO), and P•Zn_2 (CzrA•Zn_2), with only the doubly ligated complex, P•Zn_2•D (CzrA•Zn_2•CzrO) not yet characterized (Figures 1b-2).[12,15] This work provides the context of the studies reported here and reaches three major conclusions. The first is that the P and P•Zn_2 states differ primarily in their dynamics: Zn^{2+} binding to the allosteric sites rigidifies backbone motions over a range of timescales, findings consistent with the idea that Zn^{2+} narrows the population distribution of CzrA dimers that collectively have low affinity for DNA. The second finding is that the DNA-bound conformation of CzrA, P•D, differs radically from the either the structure of the apo- and Zn_2 states. Thirdly, a comparison of the dynamics "fingerprints" of the DNA-bound vs. Zn_2-bound CzrAs vs. a common reference state, apo-CzrA, reveals that the two ligand binding sites are dynamically linked, *i.e.*, CzrO binding induces long-range motional disorder into the allosteric sites, while Zn^{2+} binding *reduces* the backbone motions of the DNA binding interface, far from the first coordination shell of the metal.

In this work, we address the degree to which these dynamical and structural differences impact the global thermodynamics of both homotropic and heterotropic allosteric linkages. We find that the dynamic rigidification observed previously by NMR[12,15] occurs largely upon filling the second site on apo-CzrA, and that this defines the origin of the strong negative homotropic cooperativity of metal binding. In contrast, global rigidification fails to occur in the P•D complex on Zn^{2+} binding, which gives a net positive allosteric coupling entropy, ΔS_c. These findings are the first to elucidate the energetics of allosteric metalloregulation for any metal sensor protein, and provide a perfectly general thermodynamic framework with which to investigate other metal and oxidative stress sensing repressors, in particular those that are positively activated by inducer recognition.[11,22]

Results

Coupled equilibrium model

The linked equilibrium scheme that fully describes the degree to which Zn^{2+} regulates the binding of the apo-CzrA homodimer (CzrA) to the 28-bp CzrO DNA harboring a single 12-2-12 inverted repeat is shown in Figure 2. Previous studies reveal that that apo-CzrA forms a high affinity 1:1 dimer:DNA complex on this DNA.[15] The CzrA monomer-dimer equilibrium is not explicitly indicated in this model; however, under solution conditions used to measure Zn^{2+} binding equilibria (50–100 μM CzrA monomer, pH 7.0), apo-CzrA is greater than 95% dimeric.[23] The strategy used here was to resolve as many K_i as possible using isothermal titration calorimetry (ITC) which, in turn, permits a determination of all of the relevant linkage relationships in this system. The overall coupled equilibrium constant, defined by K_c^t, is dictated by the equilibrium shown in Figures 1b and 2, with the overall heterotropic coupling energies, ΔG_c^t, ΔH_c^t and ΔS_c^t, thermodynamic state functions defined by eqs 2–4:

$$\Delta G_c^t = -RT\ln(K_5K_6/K_1K_2) = -RT\ln(K_4/K_3) \quad (2)$$

$$\Delta H_c^t = (\Delta H_5 + \Delta H_6) - (\Delta H_1 + \Delta H_2) = \Delta H_4 - \Delta H_3 \quad (3)$$

$$\Delta S_c^t=(\Delta S_5+\Delta S_6)-(\Delta S_1+\Delta S_2)=\Delta S_4-\Delta S_3 \quad (4)$$

The coupled equilibrium shown can also be divided into two step-wise coupled equilibria which define the successive binding of the first (Zn_1) and second (Zn_2) ions to the dimer relative to the apo-CzrA and Zn_1-CzrA reference states, respectively (enclosed by the *yellow* and *green* boxes, respectively, Figure 2). Analogous step-wise heterotropic coupling energies, ΔG_c^i, ΔH_c^i and ΔS_c^i (where i=1 or 2) are then defined by eqs 5–10

$$\Delta G_c^1=-RT(K_5/K_1)=-RT(K_7/K_3) \quad (5)$$

$$\Delta H_c^1=\Delta H_5-\Delta H_1=\Delta H_7-\Delta H_3 \quad (6)$$

$$\Delta S_c^1=\Delta S_5-\Delta S_1=\Delta S_7-\Delta S_3 \quad (7)$$

$$\Delta G_c^2=-RT(K_6/K_2)=-RT(K_4/K_7) \quad (8)$$

$$\Delta H_c^2=\Delta H_6-\Delta H_2=\Delta H_4-\Delta H_7 \quad (9)$$

$$\Delta S_c^2=\Delta S_6-\Delta S_2=\Delta S_4-\Delta S_7 \quad (10)$$

with the sum of the step-wise coupling energies equal to the total coupling energies. In previous work, estimates of ΔG_c^t were determined from fluorescence polarization experiments of K_3 and K_4 (*i.e.,* the *vertical* equilibria) according to eq 2 and ranged from 5.5 to 6.3 kcal mol^{-1}.[13,14] In this work, we use ITC to measure step-wise metal binding to CzrA vs. the CzrA•CzrO complex in order to investigate in detail the energetics of metal binding as defined by the two *horizontal* equilibria (K_1, K_2, K_5 and K_6) as well as CzrA binding to the CzrO (K_3); these data are then used to extract ΔG_c^t, ΔH_c^t and ΔS_c^t.

Zn^{2+} binding to the apo-CzrA homodimer

It has previously been reported that the CzrA dimer binds two equivalents of Zn^{2+} per homodimer with step-wise affinities for the first and second Zn^{2+} ions of ~10^{12} and ~10^{10} M^{-1}, respectively.[12–14] As expected from these K_i, a direct titration of Zn^{2+} into the CzrA homodimer resulted in a step function at n = 2; this result was further complicated by visible precipitation at these CzrA concentrations (100 μM monomer; ≥99% dimer[23]), likely due to adventitious metal binding to surface sites (data not shown). We therefore implemented competition experiments using nitrilotriacetic acid (NTA) ($K_{Zn\text{-}NTA}$ = 4.57 × 10^{10} M^{-1} and β_2 = 1.74 × 10^{14} M^{-2}) to bring the observed binding constants within a measurable range as well as inhibit adventitious metal binding. Figure 3 shows a representative titration of 1.17 mM Zn^{2+} into 38 μM CzrA dimer in 50 mM Hepes, 400 mM NaCl and 3 mM NTA at 25.0 °C. Although significantly far from ideal conditions, the high monovalent salt concentration

was necessary to maintain identical solution conditions used in previous studies[13,14] and other calorimetric experiments that follow (see below). These data were fit to both two-site sequential binding and two independent site models (Figure S1, Supporting Information); the average uncorrected best fit parameters from multiple experiments are compiled in Table 1 and Table S1 (Supporting Information). Although the values for these two fitting models converge, the sequential model more accurately describes the chemical system (*i.e.* the two binding sites are not independent) and the values determined from this model were used. Under these conditions, the uncorrected $K_1 \approx 20*K_2$ and, as suggested by the raw data, the second binding event is characterized by a significantly larger binding enthalpy than the first (−6 kcal mol^{-1} vs. −3 kcal mol^{-1}) (Table 1).

Corrections of the Zn^{2+}-binding equilibria for proton displacement and NTA competition

ITC is a bulk thermodynamic method that measures the global heat of a reaction. In the case of metal-protein interactions, the displacement of protons from protein ligands upon metal binding and subsequent protonation of the buffer can contribute significantly to the observed enthalpy from eq 11.

$$Zn^{2+} + H_n{}^{+}CzrA + n\text{Buffer} \rightleftharpoons Zn \bullet CzrA^{2+} + n\text{H} - \text{Buffer}^{+} \quad (11)$$

Since the goal of this study is to determine the global thermodynamics of the interaction of metals with protein not complicated by other chemical equilibria, the heat of proton-buffer interaction must be removed from the thermodynamic cycle to generate the desired eq 12.

$$Zn^{2+} + H_N{}^{+}CzrA \rightleftharpoons Zn \bullet CzrA^{2+} + N_H H^{+} \quad (12)$$

An accurate subtraction of the net buffer protonation enthalpy is dependent on the number of protons displaced (N_H). To determine this value, titrations of Zn^{2+} into apo-CzrA were conducted under identical solution conditions except the buffer was changed to ACES, Mops or Bis-Tris in order to vary the buffer ionization enthalpy (ΔH_{buff}). The overall equilibrium is then described by eq 13:

$$Zn(NTA) + H_n{}^{+}CzrA + (n-y)\text{Buffer} \rightleftharpoons Zn \bullet CzrA^{2+} + H_yNTA + (n-y)\text{H} - \text{Buffer} \quad (13)$$

Control titrations of Zn^{2+} into NTA under identical conditions (Table S2, Supporting Information) provide the relevant background heats generated by NTA protonation upon metal transfer to CzrA. After correction for NTA-buffer interactions (see Materials and Methods), the observed calorimetric enthalpies, ΔH_{cal}, are plotted vs. buffer ionization enthalpies according to the linear relationship

$$\Delta H_{cal} = N_H \Delta H_{buff} + \Delta H_{int} \quad (14)$$

where N_H is the number of protons displaced and ΔH_{int} is the intrinsic heat associated with Zn^{2+} binding to CzrA under these condition (*i.e.* eq 12).

NTA-corrected K_i for Zn^{2+} binding to the CzrA homodimer (pH 7.0, 25.0 °C) are K_1=1.2 × 10^{12} M^{-1} and K_2=6.0 × 10^{10} M^{-1} at pH 7.0 (Table 2). Each of these values agree well with the

spectroscopically determined values of 2.5×10^{12} M^{-1} and 3.4×10^{10} M^{-1}.[13] Figure 4 shows the linear dependence of the ΔH_{cal} on $\Delta H_{H\text{-}Buff}$ after correction for competition by NTA. The best fits to these data result in $N_H \approx 1.0$ for the binding of each Zn^{2+} ion, revealing on average, two net protons or 1 per site, released on formation of the Zn_2-CzrA homodimer complex. The resulting values of ΔH_{int} for the first and second Zn^{2+} binding events, ΔH_1 and ΔH_2, are ~0 and −2.9 kcal mol^{-1}, respectively, revealing greater enthalpic driving force for the second Zn^{2+} binding as compared to the first. However, Zn^{2+} binding to the dimer is most strongly favored entropically, and far more so for the first relative to the second Zn^{2+} (Table 2; $-T\Delta S_1 = -16.6$ kcal mol^{-1} K^{-1} and $-T\Delta S_2 = -11.9$ kcal mol^{-1} K^{-1}); this gives rise to a homotropic coupling free energy of ≈+1.8 kcal mol^{-1} (Table 3).

Temperature dependence of Zn^{2+} binding to the apo-CzrA homodimer

A large change in the molar heat capacity upon ligand binding, ΔC_p, are often indicative of a structural rearrangement due to the hydrophobic effect.[24] To determine ΔC_p, ΔH_1 and ΔH_2 were measured by ITC by conducting identical titrations (50 mM Hepes, 400 mM NaCl and pH 7.0) of Zn^{2+} into CzrA at 15 °C, 25 °C and 35 °C. These data were all fit to the same two-site sequential model (Table 1) and the NTA- and buffer ionization enthalpy-independent values were calculated (Table S3, Supporting Information). Plots of ΔH_i vs. temperature are linear and give $\Delta C_p{}^1 = -230 \pm 10$ cal mol^{-1} K^{-1} and $\Delta C_p{}^2 = -110 \pm 10$ cal mol^{-1} K^{-1} (Figure 5). Although the crystallographic structure of apo-CzrA does not markedly differ from that of Zn_2 CzrA,[12] the magnitude of $\Delta C_p{}^i$ suggests that metal binding may induce a modest change in structure (*vida infra*), a finding consistent with the fact that ^1H-^{15}N HSQC spectra of apo- and Zn_2-CzrA are readily distinguished from one another in solution.[14,25] However, a high resolution solution structure of apo-CzrA remains unavailable.

CzrA dimer binding to the CzrO DNA

ITC titrations were next carried out to investigate the thermodynamics of the binding of the CzrA homodimer to 28-bp DNA operator, CzrO (*blue* dashed box, Figure 2). Previous studies with longer DNA duplexes containing a single core TGAAxxxxxxTTCA sequence with a 12-2-12 inverted repeat (41 and 56 bps) revealed the presence of multiple additional lower affinity binding sites even at 0.4 M NaCl.[13,14,23] However, recent spectroscopic studies reveal that a 28-bp duplex contains all of the information required to form a high affinity complex,[15] and this DNA was used for all thermodynamic experiments. Figure 6 shows a representative titration of 500 μM CzrA homodimer into 10 μM CzrO under solution conditions identical to those used previously (50 mM Hepes, 400 mM NaCl, pH 7.0 and 25.0 °C).[13] Unexpectedly, we observe two binding events that can be fit to a two-site sequential model defined by a high affinity site ($K_1 = 2 \times 10^8$ M^{-1}, $\Delta H_1 = -7.4 \pm 0.2$ kcal mol^{-1}) at the stoichiometric equivalence point and a lower affinity site ($K_2 = 1.2 \times 10^6$ M^{-1}, $\Delta H_2 = -2.3 \pm 0.4$ kcal mol^{-1}) corresponding to the weaker binding of a second CzrA dimer to the duplex (Table 1). Note that K_1 and K_2 correspond to K_3 and K_{3a} in Figure 2.

At the protein concentrations used in this titration, particularly during the initial injections in which the total CzrA concentration is <10 μM, the CzrA monomer–dimer equilibrium ($K_{dimer} = 1.7 \times 10^5$ M^{-1})[23] is linked to that of the dimer-CzrO binding equilibrium, *i.e.*, non-negligible CzrA monomer is present under these conditions. If not explicitly considered, this would underestimate the true value of the CzrA dimer binding affinity. To model this, we used DynaFit[26] to simulate a titration of apo-CzrA into CzrO using identical macromolecule concentrations and K_i values determined by ITC. This simulated curve was then fit to a binding model that incorporates K_{dimer} (Figure S2, Supporting Information) and K_1 (K_3 in Figure 2) and K_2 (K_{3a}) were determined to be 1.3×10^{11} M^{-1} and 6.2×10^8 M^{-1}, respectively. Both are in good agreement with spectroscopically determined values of ≈4×10^{11} M^{-1} and 1×10^9 M^{-1}, respectively.[13,15] All heat generated from a shift in the monomer–dimer equilibrium that

occurs upon injection of a concentrated solution of apo-CzrA into the much more dilute reaction cell should be cancelled by the reformation of the dimer upon binding to CzrO; as a result, no correction of the ΔH term is necessary.

Zn^{2+} binding to the apo-CzrA•CzrO complex

In order to determine the overall coupling energetics (eqs 2–4), we next determined K_5 and K_6 (Figure 2), the step-wise affinities of a preformed apo-CzrA dimer•CzrO complex for Zn^{2+}. A representative titration of 1.15 mM Zn^{2+} into a 28 μM CzrA dimer•CzrO complex (32 μM CzrO was used to ensure a 1:1 dimer:DNA complex) is shown in Figure 7. This experiment was performed in the presence of 10 mM imidazole to inhibit complex precipitation as a result of adventitious metal binding, an ideal choice given that it provides a very weak competition at this concentration and pH. A correction factor of 2.3 was determined by conducting Zn^{2+} → NTA titrations in the presence and absence of imidazole (Table S2, Supporting Information), in good agreement with the calculated value of ~6 for Zn^{2+}-imidazole interactions under these conditions.

As found for the titrations of Zn^{2+}into apo-CzrA, these data, as expected, show two clear binding events, with a major inflection occurring at $n = 2$ (Figure 7). A sequential two site model fails to generate a reasonable fit to the data (Figure S1b and Table S2, Supporting Information). A two-site model in which the stoichiometry (n_i) of the two steps was allowed to vary gives $n_1 \approx 0.8$ and $n_2 \approx 1.2$, with the cumulative stoichiometry, $n_1 + n_2$, the expected value of 2. This reveals 100% occupancy of that both metal sites on the complex at the end of the titration. Although close to the expected values of $n_1 = n_2 \approx 1.0$, fits constrained by $n_1 = n_2 \approx 1.0$ resulted in significantly poorer fits to the data (Figure S1, Supporting Information). One possible explanation of the non-integer stoichiometry ultimately ruled out is that the kinetics of the first metal binding event are slow and this isotherm reflects a non-equilibrium titration. However, a titration with a longer interval between injections (10 min) showed no significant difference in the binding profile (data not shown). A very similar binding profile was also obtained when the concentration of CzrA-CzrO complex was nearly doubled (Figure S3, Supporting Information), thus revealing that small amounts of unbound Zn_2-CzrA are not present in these mixtures at the end of the titration, and thus cannot influence the shape of the isotherm or the measured stoichiometries. This was further confirmed by a gel filtration experiment, in which a post-titration ITC sample was subjected to chromatography. This sample revealed comigration of the CzrA•CzrO complex with 1.9 mol dimer•equiv Zn^{2+} (measured by atomic absorption as described in material and methods) and no detectable dissociated Zn_2 CzrA in this sample (Figure S4, Supporting Information). Table 1 summarizes the average best fit uncorrected thermodynamic parameters for these data.

To complete the thermodynamic analysis of Zn^{2+} binding to the CzrA•CzrO complex, it was next necessary to determine the number of protons displaced upon metal binding to the complex. Additional titrations of Zn^{2+} into preformed CzrA•CzrO complexes were carried out in Mops, ACES and Bis-Tris under otherwise identical conditions (Table S3, Supporting Information). Figure 4 again shows a linear dependence of ΔH_{cal} on $\Delta H_{H\text{-}Buff}$ with best fits of $N_{H1} = 1.4 \pm 0.1$ and $N_{H1} = 0.64 \pm 0.07$ for each of the two Zn^{2+} ions, with a net proton displacement of ≈2, identical to that measured for the binding of Zn^{2+} to the unbound apo-CzrA dimer. Table 2 shows the corrected Zn^{2+} binding thermodynamic parameters. Strikingly, Zn^{2+} binding to CzrA•CzrO complex is characterized by small *endothermic* enthalpies ($\Delta H_5 \approx \Delta H_6 \approx 3.0$ kcal mol^{-1}) superimposed on a strong entropic driving force at each step ($-T\Delta S_5 = -16.1$ kcal mol^{-1} K^{-1} and $-T\Delta S_6 = -15$ kcal mol^{-1} K^{-1}) (Table 2).

Coupling Energies

As pointed out above, the linked equilibrium scheme (Figures 1b-2) is governed by three overall heterotropic coupling energies, ΔG_c^t, ΔH_c^t and ΔS_c^t defined by eqs 2–4 which collectively characterize the equilibrium reaction shown in eq 15:

$$(Zn^{2+})_2CzrA+CzrA \bullet CzrO \rightleftharpoons (Zn^{2+})_2CzrA \bullet CzrO+CzrA \quad (15)$$

As for any free energy cycle of this kind, coupling energies can be taken from the difference between the DNA binding energies of Zn_2•CzrA (K_4) relative to apo CzrA (K_3; the *vertical* equilibria; Figure 1a, Figure 2) or the Zn^{2+} binding energies of CzrA•CzrO complex (defined by K_5 and K_6) relative to the apo-CzrA (defined by K_1 and K_2; the *horizontal* equilibria). Since we have all of the thermodynamic information required for the coupling analysis using the horizontal equilibria, this approach was used here. Analogous expressions (eqs 5–10) are given for the two step-wise binding energetics (Zn_1 and Zn_2) which must sum to the total values.

Table 3 summarizes the average step-wise (Zn_1 and Zn_2) and net heterotropic thermodynamic coupling energies and these are shown graphically in Figure 8. The overall coupling free energy, ΔG_c^t, is 6.3 kcal mol^{-1}, a value consistent with allosteric negative regulation of CzrO binding by Zn^{2+} and in excellent agreement with previously determined values measured from the *vertical* equilibria in Figure 2b.[13,14] The enthalpic component of the coupling energy, ΔH_c^t = 9.4 kcal mol^{-1}, is of the same sign as ΔG_c^t and compensates for an opposing entropic component, $-T\Delta S_c^t$ = −3.0 kcal mol^{-1}, *i.e.*, ΔS_c^t is *positive*. Each Zn^{2+} ion contributes nearly equally ($\Delta G_c^1 = \Delta G_c^2 \approx 3$ kcal mol^{-1}) to the net coupling free energy, but the underlying energetics are dramatically different. Formation of the Zn_1 complex is characterized by a smaller enthalpic coupling component relative to formation of the Zn_2 complex from the Zn_1 state, $\Delta H_c^1 = 2.9 \pm 0.4$ kcal mol^{-1} compared to $\Delta H_c^2 = 6.5 \pm 0.3$ kcal mol^{-1}, a difference of which is largely offset by a *positive* ΔS_c associated with filling the second site with metal, *i.e.*, $-T\Delta S_c^2 \approx -T\Delta S_c^t$, since $-T\Delta S_c^1 \approx 0$ (Figure 8).

Zn^{2+} binding to both the apo-CzrA homodimer and the apo-CzrA dimer•CzrO complex is characterized by negative homotropic cooperativity in both cases, *i.e.*, $K_1 > K_2$ and $K_5 > K_6$ (Figure 2;) and $\Delta(\Delta G) > 0 \approx 1.8$ and 1.3 kcal mol^{-1}, respectively (Table 3). In both cases, negative homotropic allostery is entropically driven, $\Delta(-T\Delta S) > \Delta(\Delta H)$, but far more so for the binding of Zn^{2+} to the free apoprotein relative to the protein-DNA complex (Table 3).

Discussion

In this study, we have employed equilibrium isothermal titration calorimetry to measure the thermodynamic underpinnings of allosteric negative regulation of specific CzrO binding by the zinc-sensing homodimeric repressor, CzrA. These global thermodynamics are discussed in the context of known structural and dynamics studies of the four allosteric end-states, apo CzrA (P), apo-CzrA•CzrO (P•D), Zn_2CzrA (P•Zn_2) and Zn_2CzrA•CzrO (P•Zn_2•D) (Figures 1–2).[12,15] We first focus our discussion on the two horizontal Zn^{2+} binding equilibria individually (Figure 2), and then discuss the step-wise homotropic and heterotropic coupling energies derived from this analysis and point out the essentiality of both entropic and enthalpic components to zinc sensing by CzrA.

Entropy-driven zinc binding to CzrA

All Zn^{2+} binding equilibria (K_1, K_2, K_5, K_6) are dominated by a large global entropic component (Table 2). These observations are consistent with previously reported investigations of Zn^{2+} binding to other biological macromolecules, after correction to pH 7.0 and subtracting the

effects of competing equilibria. For example, the binding of Zn^{2+} to the peripheral site of *K. aerogenes* UreE, the metallochaperone responsible for loading Ni^{2+} into urease, is characterized by $\Delta G = -12.2$ kcal mol^{-1} and $-T\Delta S = -8.3$ kcal mol^{-1}.[27] Zn^{2+} binding to a histidine-rich decapeptide (PHGHGHGHGP, called IRTpep) occurs with $\Delta G = -9.4$ kcal mol^{-1} and a $-T\Delta S = -11.0$ kcal mol^{-1}, that compensates for the endothermic enthalpy change.[28]

Four typical contributors to the entropy term in transition metal complex formation are (1) formation of metal coordination bonds, (2) displacement of water molecules from the solvated metal ion, (3) displacement of the solvation shell surrounding the ligand (or protein), and (4) imposed conformational restraints.[28] Since the net number of protons displaced upon Zn^{2+} association is ~1 at pH 7.0 and four coordination bonds are formed in each case (for UreE, 2 His and 2 buffer molecules make the four-coordinate complex), the net solvent rearrangement around the Zn^{2+} and H^+ release are similar in each system; as a result, the net contribution of components (1) and (2) listed above should be reasonably similar in all three systems. IRTpep is an unstructured peptide in the absence of metal, and in this regard differs most strongly from CzrA. IRTpep clearly loses significant conformational flexibility upon metal binding relative to apo-CzrA, since at least three of the four coordinating residues in CzrA (D84, H86, and H97′; H100′ may well fold in on metal binding)[12] form a comparatively preformed ligand binding site. This predicts that the net entropy term, $-T\Delta S$, will be less negative for IRTpep than for CzrA, which is exactly what we find (Table 2). Therefore, one likely origin of the additional entropic driving force in the binding of Zn^{2+} to apo-CzrA relative to IRTpep derives from component (4), a difference in conformational restraints imposed upon metal binding.

Homotropic Allostery

Zn^{2+} binding to the apo-CzrA homodimer is characterized by an entropically favored ($\Delta(-T\Delta S) = 4.7$ kcal mol^{-1}) negative cooperativity, $\Delta(\Delta G) = 1.8$ kcal mol^{-1} that is enthalpically opposed ($\Delta(\Delta H) = -2.9$ kcal mol^{-1} (Table 3). The negative cooperativity and underlying energetics bear striking parallels to the binding of two cAMPs to the N-terminal regulatory domain dimer of *E. coli* CAP (catabolite activator protein) where ΔH_2 was found to be more negative than ΔH_1 by 1.1 kcal mol^{-1}, with $-T\Delta S_2$ less negative than $-T\Delta S_1$ by ≈4 kcal mol^{-1}.[3] In the cAMP-CAP system, $1(\Delta G) = 2.8$ kcal mol^{-1}, or nearly twice that of Zn^{2+} binding to CzrA (Table 3), and this homotropic allostery was proposed to manifest in CAP by dynamic differences at all timescales.[3] More recent work documents a coil-to-helix transition on cAMP binding to the unliganded intact CAP dimer[29] and this suggests that some structural ordering may contribute to the unfavorable entropy term, perhaps associated with formation of the $cAMP_2$ state relative to the $cAMP_1$ state.

Although the conformational dynamics of the Zn_1CzrA intermediate have not been investigated, a comparison of the Zn_2 and apo end states reveals multiple potential dynamical contributors to the different global entropies measured for loading the first vs. the second Zn^{2+} ion on the dimer.[15] For example, small differences in the residue-specific backbone order parameters, S^2, suggest a lower backbone conformational entropy of the Zn_2 vs. the apo-state, both of which are potential contributor to ΔC_p[24] and negative cooperativity of ligand binding.[3] There may also be a detectable quenching of the internal dynamics at intermediate timescales on Zn^{2+} binding as evidenced by the larger number of residues exhibiting conformational exchange broadening in apo-CzrA relative to Zn_2 CzrA.[15] In addition, Zn^{2+} globally stabilizes the native-state conformational ensemble as determined by an overall decrease in hydrogen-deuterium exchange rates, at least in the core of the molecule.[12,15]

The magnitude of the overall heat capacity change on Zn^{2+} binding to apo-CzrA, $\Delta C_p^t = -340$ cal mol^{-1}K^{-1} is consistent with a small structural reorganization in the dimer superimposed on a net disordering of water molecules at the metal binding sites.[24,30–32] This is in accord

with the fact the global solution structures of apo-CzrA and Zn_2 CzrA are likely more similar than different.[12,15] The relative magnitudes of ΔC_p^1 vs. ΔC_p^2 would suggest that the first Zn^{2+} binding event triggers a somewhat larger structural change in the apoprotein while introducing structural asymmetry and into the dimer.[13]

In striking contrast to the free apoprotein, the step-wise ΔH_i values for Zn^{2+} binding to the CzrA•CzrO complex are both *positive* and of similar magnitude (2.9 kcal mol^{-1} and 3.6 kcal mol^{-1}, Table 2); this gives rise to a small *positive* $\Delta(\Delta H)$ and provides a contribution to $\Delta(\Delta G)$ that is equivalent to the $\Delta(-T\Delta S)$ term (0.6 kcal mol^{-1}, Table 3). Thus, although the magnitude of homotropic coupling free energy, $\Delta(\Delta G)$, for the binding of Zn^{2+} to the two sites on the protein-DNA complex is comparable to that of the apoprotein, the underlying energetics are very different. The origin of the step-wise unfavorable and endothermic ΔH values is likely dominated by a decrease in favorable contacts at what is predicted to be a well-packed and enthalpically stabilized CzrA-CzrO interface.[15] These data further suggest that the dynamics of the fully saturated Zn_2•CzrA•CzrO "ternary" complex that contribute to the entropy term may not be dampened to the same degree as Zn_2 CzrA, given the very different magnitudes of the $\Delta(-T\Delta S)$ terms in each case (Table 3). Unfortunately a high resolution structure of the Zn_2•CzrA•CzrO complex is not available. However, a ^1H-^{15}N HSQC spectrum of the complex suggests that CzrA adopts a "hybrid" structure in what is essentially a short-lived, high energy intermediate state that attempts to maximize protein-DNA and protein-Zn^{2+} interfaces.

Heterotropic coupling components

The driving force for the large overall ΔG_c^t of +6.3 kcal mol^{-1} is the large positive ΔH_c^t of 9.4 kcal mol^{-1} which is opposed by a $-T\Delta S_c^t$ of ≈ −3.1 kcal mol^{-1}, contributed nearly exclusively to the second Zn^{2+} binding step (Figure 8). The large favorable coupling enthalpy is consistent with the significant structural differences among the allosteric states along the bottom vs. the top horizontal equilibria (Figure 2), and has been observed many allosteric proteins.[6,33] However, distinct underlying energetics characterize the two otherwise approximately equivalent ΔG_c^i (≈3 kcal mol^{-1}, Table 3 and Figure 8) revealing that the two Zn^{2+} ions function in fundamentally different ways. In the free protein, binding of the first Zn^{2+} ion drives a detectable conformational change in the dimer, while the second one dampens the internal dynamics and enhances the packing of the allosterically inhibited state. When bound to DNA, both of these processes are likely compromised, with the energetics of Zn^{2+} binding to the complex likely dominated by a sequential disruption of the protein-DNA interface on loading each metal.

The quaternary structure and dynamics "fingerprints" of apo-CzrA•CzrO differ dramatically from the allosterically inhibited Zn_2 form in solution (Figure 9).[15] In particular, the allosteric α5 helices in the CzrA-CzrO complex appear less well packed and highly dynamic over a range of timescales, with the hydrophobic core of the dimer at least partially exposed to solvent;[15] in fact, the solvent-exposed surface area in this conformation is measurably greater than in Zn_2 CzrA (neglecting the interface that interacts with the DNA) (Figure 9; Table S4, Figure S5, Supporting Information). Despite this, Zn^{2+} coordination by metal ligands in the C-terminal α5 helices occurs with a strongly favorable $-T\Delta S$ term similar to that associated with formation of the Zn_1-CzrA intermediate that is unconstrained by bound DNA (compare $-T\Delta S_1$ is close with $-T\Delta S_5$; Table 2), giving a first step-wise heterotropic coupling entropy, $-T\Delta S_c^1$, that to zero (Table 3). This indicates that the structural and dynamical foundations of the $-T\Delta S_1$ and $-T\Delta S_5$ terms may be distinct, *i.e.*, more favorable solvent reorganization at the "top" of the dimer and a loss of conformational restriction at the protein-DNA interface (resulting in a net positive ΔH_5) that more than compensates for what is likely to be significant ordering of the α5 helices upon Zn^{2+} binding to the complex. In contrast, while $-T\Delta S_6$ is less favorable for the binding of the second Zn^{2+} to the Zn_1•CzrA•CzrO complex relative to the first, it is *not*

less favorable to the same degree as in unbound CzrA. In fact, nearly the entire magnitude of the $-T\Delta S_c^t$ term derives from loading the second Zn^{2+} to the complex, *i.e.*, from $-T\Delta S_c^2$. Since all the ancillary contributions to the entropy term associated with formation of the metal-ligand bonds in CzrA (H^+ release, solvent release from the metal, etc.) essentially cancel across the top and bottom horizontal Zn^{2+} binding equilibria (Figure 2), it seems likely that the fully metallated Zn_2•CzrA•CzrO complex is significantly more conformationally dynamic than is the allosterically inhibited Zn_2-CzrA complex.

These thermodynamics of heterotropic coupling are fully compatible with simple expectations if one were to instead extract ΔH_c^t and ΔS_c^t from the two vertical, DNA binding equilibria (eq 2; Figure 2). Formation of the Zn_2•CzrA•CzrO complex from the Zn_2-CzrA complex and free CzrO DNA (K_4, Figure 2) is likely to be representative of non-specific binding, and would therefore lack typical characteristics of a well-packed protein-DNA interface. Formation of this complex may well be characterized by a small enthalpy change;[34] in fact, efforts to measure this equilibrium by ITC were not successful (data not shown), thus consistent with a very small and positive ΔH_4 (Table 3), in accord with experiment. The less stabilized protein-DNA interface, a consequence of loss of energetically important contacts, of Zn_2•CzrA•CzrO as compared to CzrA•CzrO would indeed predict additional conformational flexibility and a more favorable coupling entropy, (*i.e.* $\Delta S_c^t > 0$).

Summary

The thermodynamic approach we outline here is general and provides a means to elucidate the energetics of metalloregulation by other ArsR family sensors characterized by far smaller coupling free energies than CzrA,[21,35] as well as other metal-activated repressors including NikR,[36] Fur-family,[37,38] DtxR family[39,40] repressors. Here, structural studies suggest that metal-dependent narrowing of the native-state conformational ensemble[29] may be of primary importance in ligand-activated operator-promoter binding. In the specific case of *S. aureus* CzrA, we show that the negative cooperativity of Zn^{2+} binding to apo-CzrA is governed by primarily by entropy and can be rationalized on the basis of sizable changes in protein dynamics superimposed on a corresponding small structural change.[32] In striking contrast, the large enthalpic contribution to the heterotropic coupling free energy is consistent with a more dogmatic model of protein allostery, which posits that a quaternary structural change in an oligomeric protein drives biological regulation,[33] a view fully compatible with solution structural studies of CzrA.[15] However, the net positive entropic component of the heterotropic coupling free energy is also critical to the global regulatory scheme since the intrinsic disorder of the allosteric sites in the CzrA•CzrO complex[15] may lower the barrier to Zn^{2+} binding[41] while creating a high energy Zn_2•CzrA•CzrO complex poised to disassemble into Zn_2•CzrA and free CzrO. It will be interesting to determine the degree to which occupancy of both sites by Zn^{2+} is required for transcriptional derepression in the cell.[42]

Materials and Methods

Buffers and Reagents

Hepes (4-(2-hydroxyethyl)-1-piperazineethanesulfonic acid), Mops (3-(N-Morpholino) propanesulfonic acid), BisTris (2-(bis(2-hydroxyethyl)amino)-2-(hydroxymethyl) propane-1,3-diol) and Aces (2-(carbamoylmethylamino)ethanesulfonic acid) were obtained from VWR or Sigma and were prepared using Milli-Q deionized water (>18 MΩ). All chromatography materials were from GE Biosciences. Ultrapure $Zn(SO_4)$ was obtained from Alfa Aesar. A self-complementary 28-nucleottide DNA (IDT) based on the native *czr* operator promoter region, 5′-TAACATA**TGAA**-CATATG**TTCA**TATGTTA containing the conserved 12-2-12 inverted repeat (underlined) was purified on an Äkta 10 purifier using a

Source 15Q column (GE Healthcare Life Sciences), and annealed, with duplex DNA further purified away from ssDNA using the same column.

Protein Purification

CzrA, expressed from a pET3a plasmid construct in a BL21 strain of *E. coli*, was purified as previously described[23] and obtained > 95% pure. Protein integrity was verified by MALDI-TOF mass spectrometry at the Indiana University Department of Chemistry Mass Spectrometry Facility on a Bruker Biflex III MALDI-TOF Mass Spectrometer. $ZnSO_4$ concentrations were verified by atomic absorption spectroscopy on a Perkin Elmer AAnalyst Spectrometer using AA standards from Alfa Aesar in the linear range from 0.1 to 0.75 ppm. Protein concentration was determined using the molar extinction coefficient at $\varepsilon_{280} = 4470\ M^{-1}\ cm^{-1}$.[43]

Isothermal Titration Calorimetry

All ITC titrations were carried out on a MicroCal VP-ITC calorimeter using ~1 mM Zn^{2+} or ~500 μM CzrA dimer in the syringe and 15–50 μM macromolecule (CzrA dimer, CzrO or CzrA•CzrO) in the reaction cell. 3–10 μL injections were made at the default rate of 2 μL per second and 240–600 s was allowed for equilibration. All reactions were conducted in at least triplicate in 400 mM NaCl at pH 7.0 in the indicated buffer and temperature. The Origin 7.0 Software package provided by MicroCal was used for all fitting procedures[44] and the appropriate chemical model is noted in the text. In some cases, nitrilotriacetic acid (NTA) was used as a strong competitor ligand for Zn^{2+} to bring the observed Zn^{2+}-CzrA binding constant into the equilibrium (non-stoichiometric) range for analysis. In order to obtain NTA-independent binding constants, the following approach was used. Briefly, the fitted K_{ITC} contains contributions from a fixed concentration of NTA (3.0 mM). Using NIST approved equilibrium constants,[45] the competition from 3.0 mM NTA can be calculated from eq 14 and used to convert K_{ITC} into K_i from eq 15.

$$K_{comp} = 1 + K_{ZnNTA} \bullet [NTA_{base}] \tag{14}$$

$$K = K_{comp} \bullet K_{ITC} \tag{15}$$

Under these conditions, K_{comp} is 1.7×10^5 and application of eq 15 generates NTA-independent values of K_1 and K_2 (Figure 2).

Supplementary Material

Refer to Web version on PubMed Central for supplementary material.

Acknowledgments

We gratefully acknowledge financial support of this work from the NIH (GM042569) and Indiana University. We also acknowledge Mr. Ian Yarbrough for assistance in preparing Figure 9 and Table S4, Supporting Information.

References

1. Monod J, Wyman J, Changeux JP. J Mol Biol 1965;12:88–118. [PubMed: 14343300]
2. Koshland DE Jr, Nemethy G, Filmer D. Biochemistry 1966;5:365–385. [PubMed: 5938952]
3. Popovych N, Sun S, Ebright RH, Kalodimos CG. Nat Struct Mol Biol 2006;13:831–838. [PubMed: 16906160]

4. Cooper A, Dryden DT. Eur Biophys J 1984;11:103–109. [PubMed: 6544679]
5. Kern D, Zuiderweg ER. Curr Opin Struct Biol 2003;13:748–757. [PubMed: 14675554]
6. Tsai CJ, del Sol A, Nussinov R. J Mol Biol 2008;378:1–11. [PubMed: 18353365]
7. Goodey NM, Benkovic SJ. Nat Chem Biol 2008;4:474–482. [PubMed: 18641628]
8. Wand AJ. Nat Struct Mol Biol 2001;8:926–931.
9. Henzler-Wildman K, Kern D. Nature 2007;450:964–972. [PubMed: 18075575]
10. Busenlehner LS, Pennella MA, Giedroc DP. FEMS Microbiol Rev 2003;27:131–143. [PubMed: 12829264]
11. Giedroc DP, Arunkumar AI. Dalton Trans 2007;29:3107–3120. [PubMed: 17637984]
12. Eicken C, Pennella MA, Chen X, Koshlap KM, VanZile ML, Sacchettini JC, Giedroc DP. J Mol Biol 2003;333:683–695. [PubMed: 14568530]
13. Lee S, Arunkumar AI, Chen X, Giedroc DP. J Am Chem Soc 2006;128:1937–1947. [PubMed: 16464095]
14. Pennella MA, Arunkumar AI, Giedroc DP. J Mol Biol 2006;356:1124–1136. [PubMed: 16406068]
15. Arunkumar AI, Campanello GC, Giedroc DP. Proc Natl Acad Sci U S A 2009;106 in press. 10.1073/pnas.0905558106
16. Kuroda M, Hayashi H, Ohta T. Microbiol Immunol 1999;43:115–125. [PubMed: 10229265]
17. Singh VK, Xiong A, Usgaard TR, Chakrabarti S, Deora R, Misra TK, Jayaswal RK. Mol Microbiol 1999;33:200–207. [PubMed: 10411736]
18. Lu M, Fu D. Science 2007;317:1746–1748. [PubMed: 17717154]
19. Montanini B, Blaudez D, Jeandroz S, Sanders D, Chalot M. BMC Genomics 2007;8:107. [PubMed: 17448255]
20. Campbell DR, Chapman KE, Waldron KJ, Tottey S, Kendall S, Cavallaro G, Andreini C, Hinds J, Stoker NG, Robinson NJ, Cavet JS. J Biol Chem 2007;282:32298–32310. [PubMed: 17726022]
21. Liu T, Chen X, Ma Z, Shokes J, Hemmingsen L, Scott RA, Giedroc DP. Biochemistry 2008;47:10564–10575. [PubMed: 18795800]
22. Giedroc DP. Mol Microbiol 2009;73:1–4. [PubMed: 19508286]
23. Pennella MA, Shokes JE, Cosper NJ, Scott RA, Giedroc DP. Proc Natl Acad Sci U S A 2003;100:3713–3718. [PubMed: 12651949]
24. Sturtevant JM. Proc Natl Acad Sci U S A 1977;74:2236–2240. [PubMed: 196283]
25. Arunkumar AI, Pennella MA, Kong X, Giedroc DP. Biomol NMR Assign 2007;1:99–101. [PubMed: 19636838]
26. Kuzmic P. Anal Biochem 1996;237:260–273. [PubMed: 8660575]
27. Grossoehme NE, Mulrooney SB, Hausinger RP, Wilcox DE. Biochemistry 2007;46:10506–10516. [PubMed: 17711301]
28. Grossoehme NE, Akilesh S, Guerinot ML, Wilcox DE. Inorg Chem 2006;45:8500–8508. [PubMed: 17029360]
29. Popovych N, Tzeng SR, Tonelli M, Ebright RH, Kalodimos CG. Proc Natl Acad Sci U S A 2009;106:6927–6932. [PubMed: 19359484]
30. Edsall JT. J Am Chem Soc 1935;57:1506–1507.
31. Chervenak MC, Toone EJ. J Am Chem Soc 1994;116:10533–10539.
32. DiTusa CA, Christensen T, McCall KA, Fierke CA, Toone EJ. Biochemistry 2001;40:5338–5344. [PubMed: 11330996]
33. Daily MD, Gray JJ. Proteins: Structure, Function, and Bioinformatics 2007;67:385–399.
34. Kalodimos CG, Biris N, Bonvin AM, Levandoski MM, Guennuegues M, Boelens R, Kaptein R. Science 2004;305:386–389. [PubMed: 15256668]
35. Wang Y, Hemmingsen L, Giedroc DP. Biochemistry 2005;44:8976–8988. [PubMed: 15966722]
36. Chivers PT, Tahirov TH. J Mol Biol 2005;348:597–607. [PubMed: 15826657]
37. Jacquamet L, Traore DA, Ferrer JL, Proux O, Testemale D, Hazemann JL, Nazarenko E, El Ghazouani A, Caux-Thang C, Duarte V, Latour JM. Mol Microbiol 2009;73:20–31. [PubMed: 19508285]

38. Traore DA, El Ghazouani A, Jacquamet L, Borel F, Ferrer JL, Lascoux D, Ravanat JL, Jaquinod M, Blondin G, Caux-Thang C, Duarte V, Latour JM. Nat Chem Biol 2009;5:53–59. [PubMed: 19079268]
39. DeWitt MA, Kliegman JI, Helmann JD, Brennan RG, Farrens DL, Glasfeld A. J Mol Biol 2007;365:1257–1265. [PubMed: 17118401]
40. Golynskiy M, Li S, Woods VL Jr, Cohen SM. J Biol Inorg Chem 2007;12:699–709. [PubMed: 17342524]
41. Hilser VJ, Thompson EB. Proc Natl Acad Sci U S A 2007;104:8311–8315. [PubMed: 17494761]
42. Eiamphungporn W, Soonsanga S, Lee JW, Helmann JD. Nucleic Acids Res 2009;37:1174–1181. [PubMed: 19129220]
43. Pace CN, Vajdos F, Fee L, Grimsley G, Gray T. Protein Sci 1995;4:2411–2423. [PubMed: 8563639]
44. MicroCal 2002, Northampton, MA
45. NIST Standard Reference Database 46, Version 7.0, 2003.

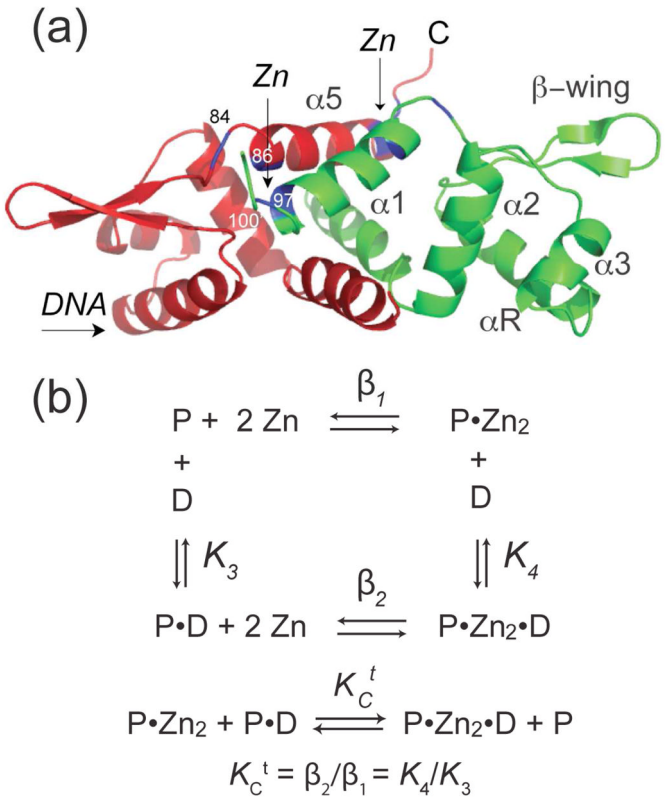

Figure 1.

(a) Ribbon diagram of Zn_2 CzrA with each monomer depicted in *red* and *green* (2KJC). The approximate positions of the Cα atoms of the α5 metal binding residues, Glu84, His86, His97′ and His100′ are highlighted on the ribbon in *blue*, and the secondary structural units are indicated on the *green* protomer. The dimer interface is made up primarily of the symmetry related α1 and α5 helices with the two metal sites bridging the α5 helical interface. The DNA binding surface is also indicated and encompasses the entire "bottom" of the molecule in this view from the β-wing tips to the α3-αR region through the N-terminal α1 helix.[15] (b) General coupling scheme where β_1 and β_2 are the overall Zn^{2+} binding affinities for the apo protein and protein-DNA complex, respectively. The allosteric coupling energies, governed by K_c^t, describe the ligand exchange reaction between the protein-DNA complex and the apo-protein.

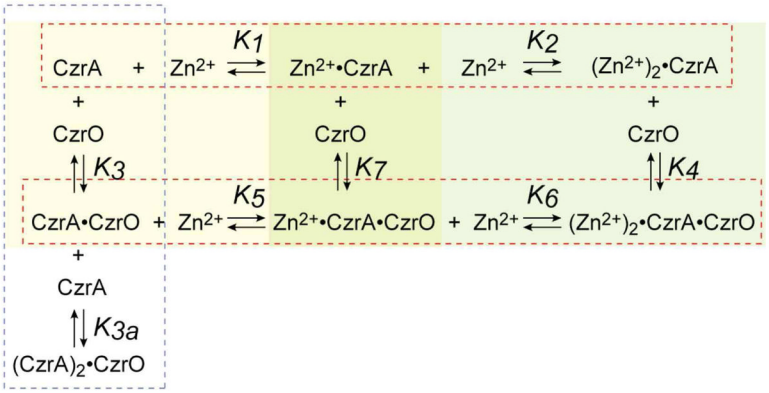

Figure 2.

Detailed thermodynamic cycle that describes the coupled equilibria considered in this study. CzrA refers to the CzrA homodimer. The *dashed-boxed* equilibria were measured directly. Step-wise coupled equilibria that describe the binding of the first and second Zn^{2+} ion to the CzrA homodimer are indicated by the *green* and *yellow* boxes, respectively. Note that the overall Zn^{2+} binding affinities, β_1 and β_2 from Figure 1b, are equal to K_1*K_2 and K_5*K_6, respectively.

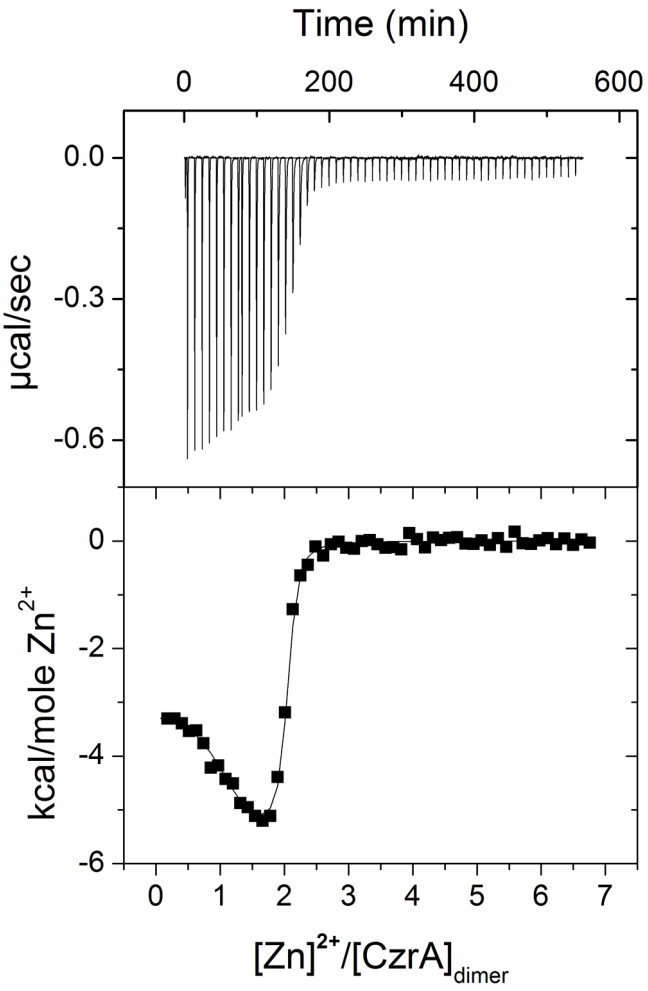

Figure 3.

Titration of 1.17 mM Zn^{2+} into 38 μM apo-CzrA dimer in 50 mM Hepes, 400 mM NaCl pH 7.0, 3.0 mM NTA and 25.0 °C. The top panel shows the raw data plotted as power vs. time and the bottom panel is the integrated, concentration normalized ITC data. The continuous line indicates that best fit according to a two-site sequential binding model. Average best fits from multiple titrations are compiled in Table 1.

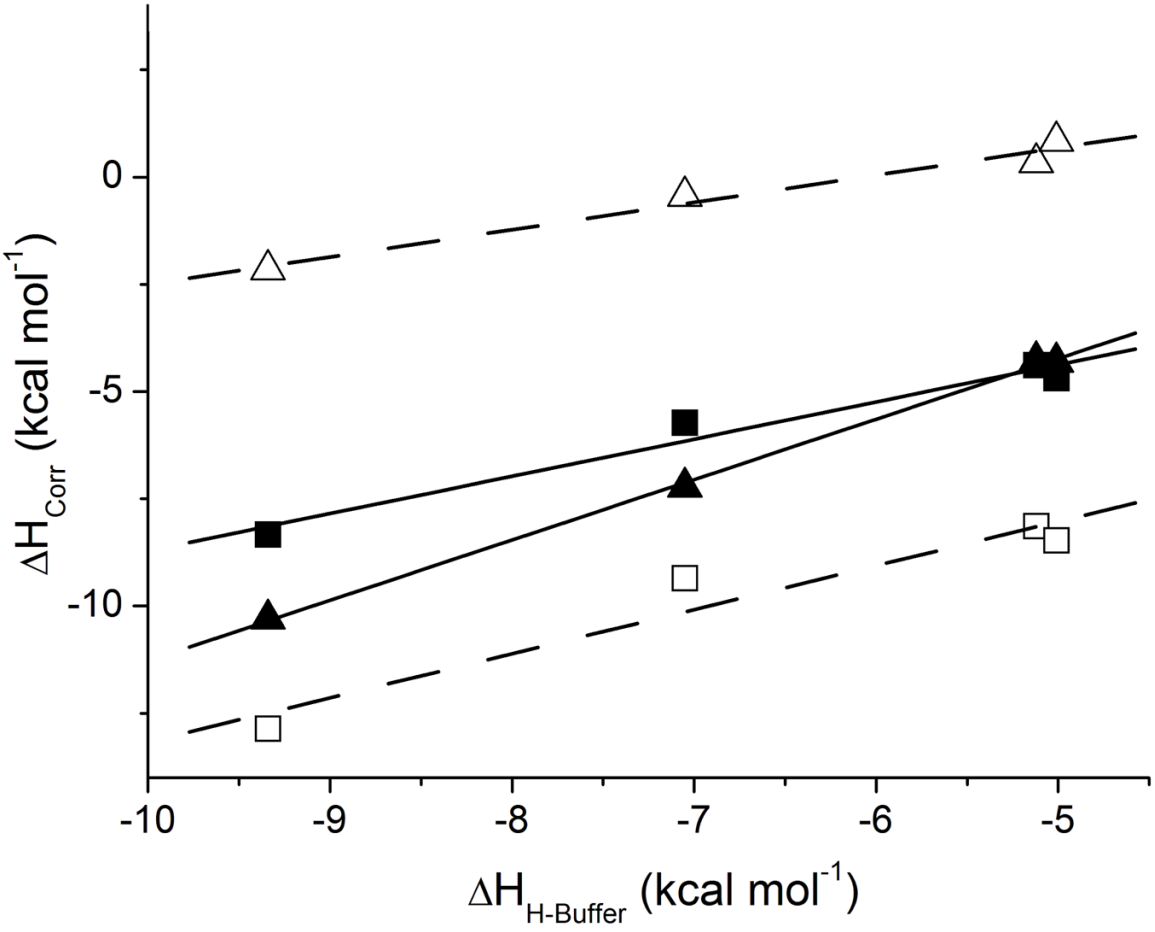

Figure 4.

Proton displacement determined by plotting the observed calorimetric enthalpy (corrected for interaction with NTA), ΔH_{corr}, plotted as a function of buffer ionization energy, $\Delta H_{H\text{-}Buffer}$. The slope of the linear relationship is the net number of protons displaced. The binding of the first Zn^{2+} (Zn_1) and second Zn^{2+} (Zn_2) ions to the apo CzrA dimer (represented by closed and open squares, respectively) displace 0.9 ± 0.1 and 1.0 ± 0.2 H^+, respectively. The analogous binding of Zn^{2+} to the CzrA•CzrO complex (closed and open triangles, respectively) displaces 1.4 ± 0.1 and 0.64 ± 0.07 H^+, respectively.

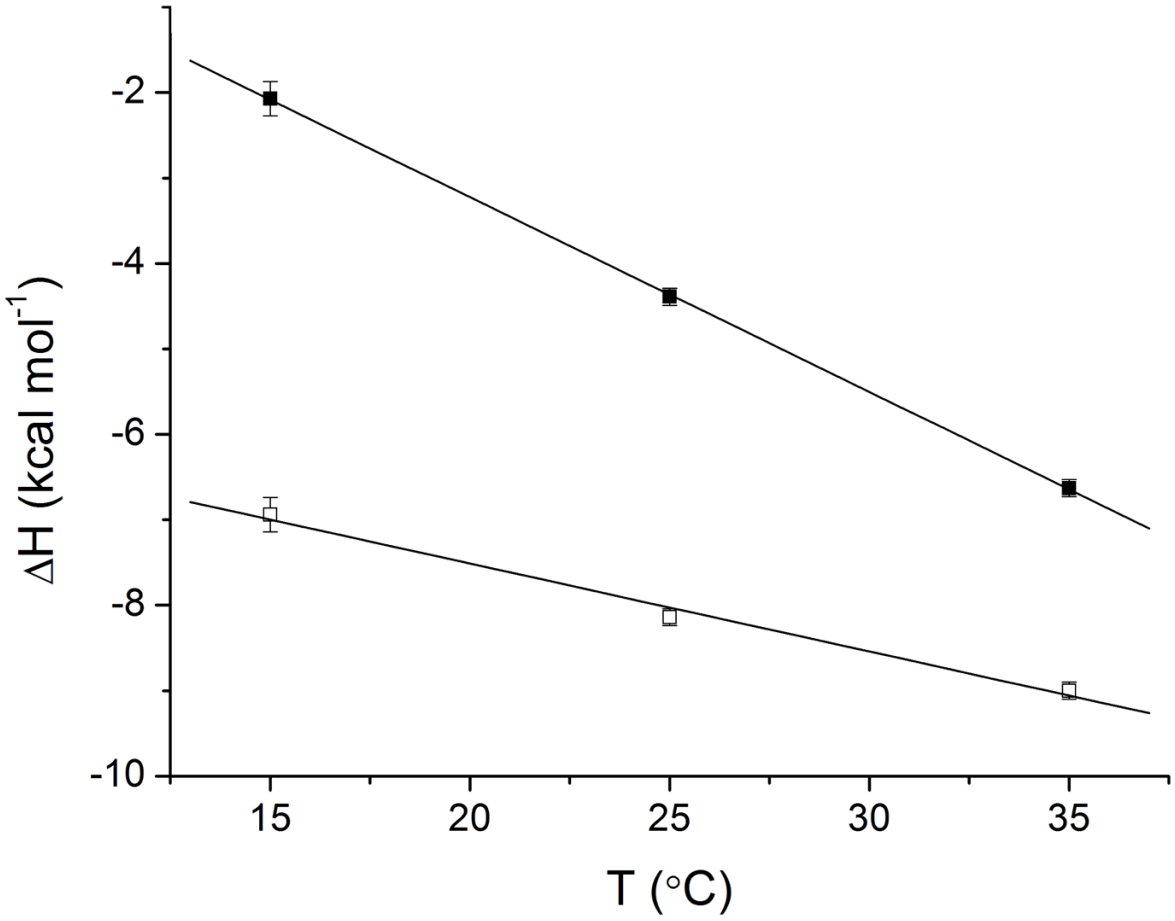

Figure 5.

Temperature-dependence of the Δ*H* for the binding of Zn^{2+} to the CzrA homodimer. *Filled squares*, binding of the first Zn^{2+} (Zn_1); *open squares*, binding of the second Zn^{2+} (Zn_2). The *black* continuous lines are linear fits that define the slope $\Delta C_p = d\Delta H/dT$. ΔC_p^1 (Zn_1) = −230 ± 10 cal $mol^{-1}K^{-1}$; ΔC_p^2 (Zn_2) = −110 ± 10 cal $mol^{-1}K^{-1}$.

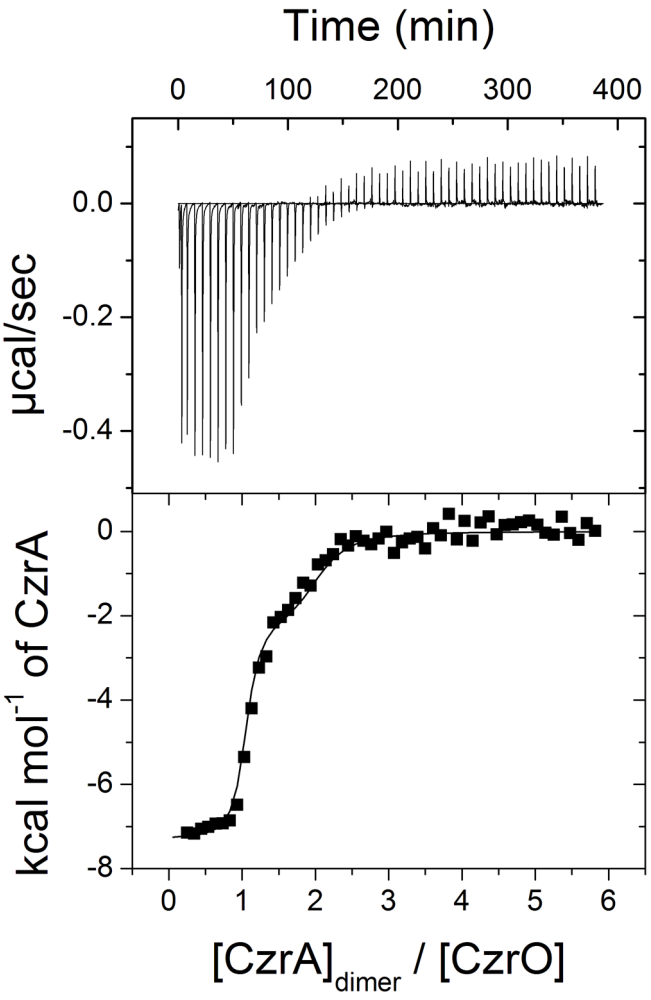

Figure 6.

Titration of 500 μM apo-CzrA dimer into 10 μM CzrO in 50 mM Hepes, 400 mM NaCl pH 7.0 and 25°C. The top panel shows the raw data plotted as power vs. time and the bottom panel is the integrated, concentration normalized ITC data. The black continuous line indicates that best fit according to a sequential binding model. Average uncorrected best fitted parameters are summarized in Table 1.

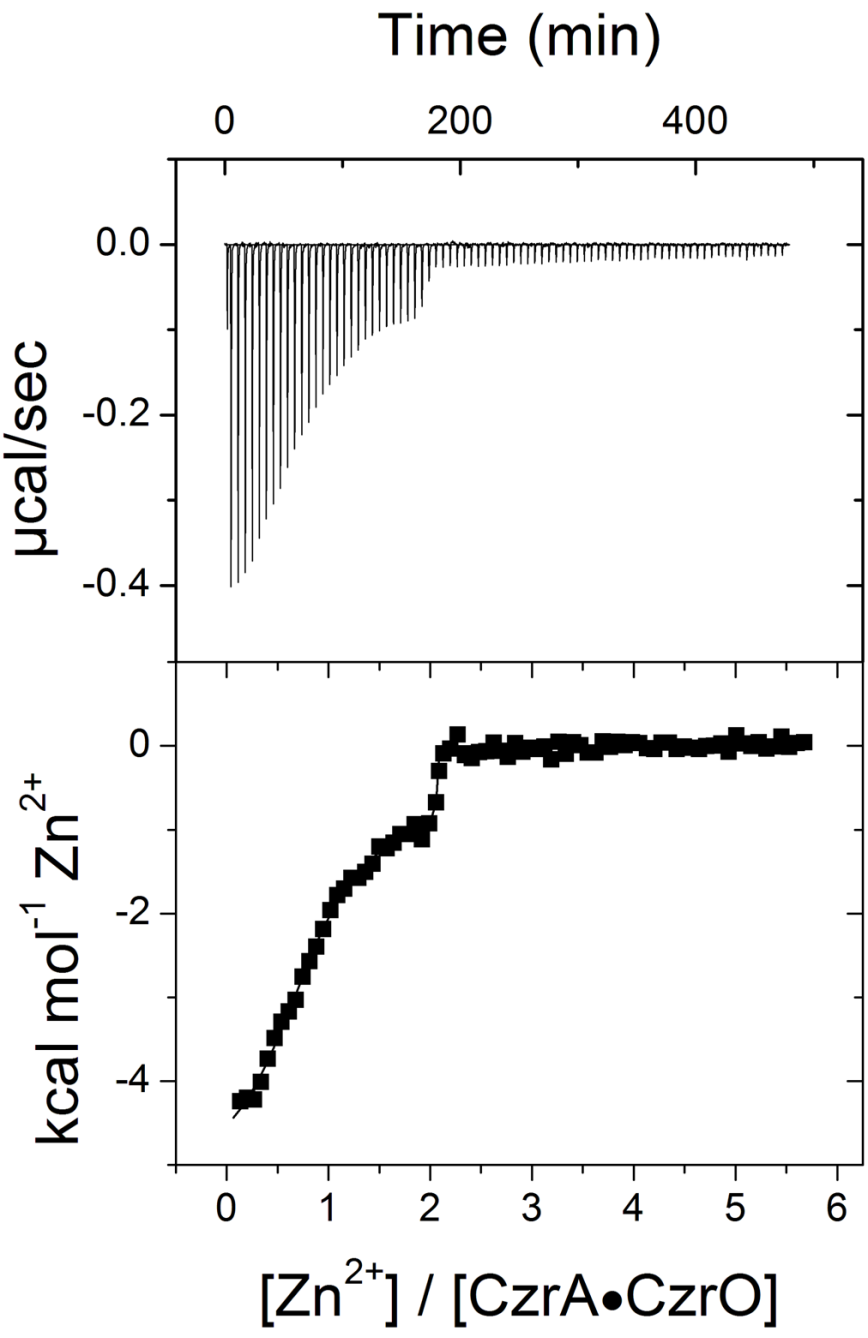

Figure 7.
Titration of 1.15 mM Zn^{2+} into 28 μM CzrA•CzrO complex with a 10% excess of CzrO in 50 mM Hepes, 400 mM NaCl, 10 mM imidazole, pH 7.0 and 25.0 °C. The top panel shows the raw data plotted as power vs. time and the bottom panel is the integrated, concentration normalized ITC data. The *black continuous* line indicates the best fit to the according to a two-site binding model. Average uncorrected best fitted parameters are summarized in Table 1.

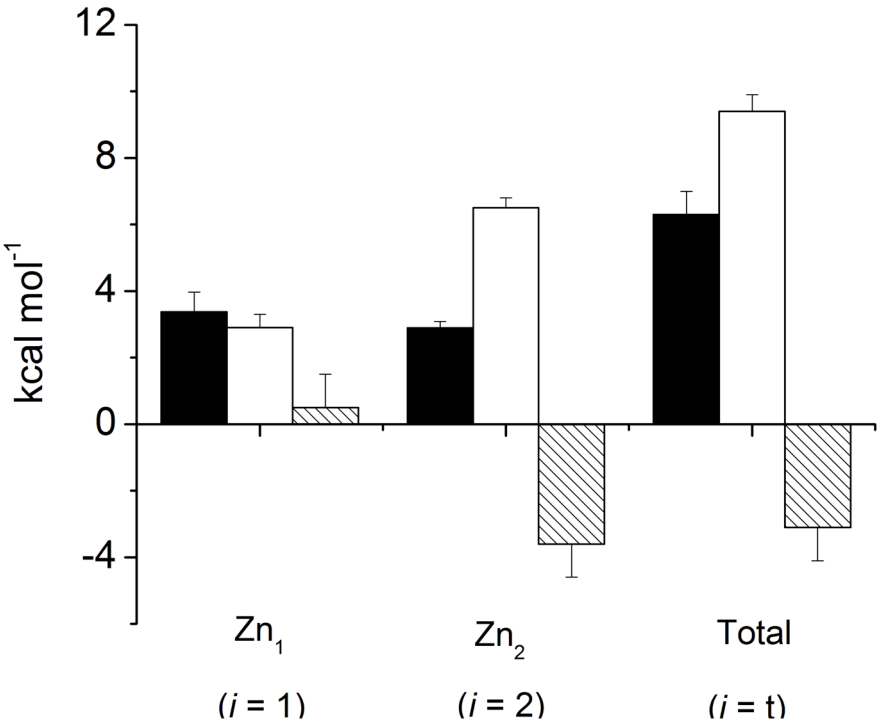

Figure 8.

Graphical representation of the net and step-wise heterotropic coupling energies for CzrA where ΔG_c^i is shown in *black bars*, ΔH_c^i is in *open bars* and $-T\Delta S_c^i$ is *stippled bars*. *i* is 1, 2 or *t* and refers to the heterotropic coupling parameters obtained for the binding of the first Zn^{2+} ion to the CzrA homodimer (*i*=1), the second metal site on the dimer relative to the Zn_1 reference state (*i*=2), and the cumulative effect of filling the both sites relative to the apo-CzrA reference state (*i*=*t*). See Figure 2 for coupled equilibrium and Table 3 for parameters.

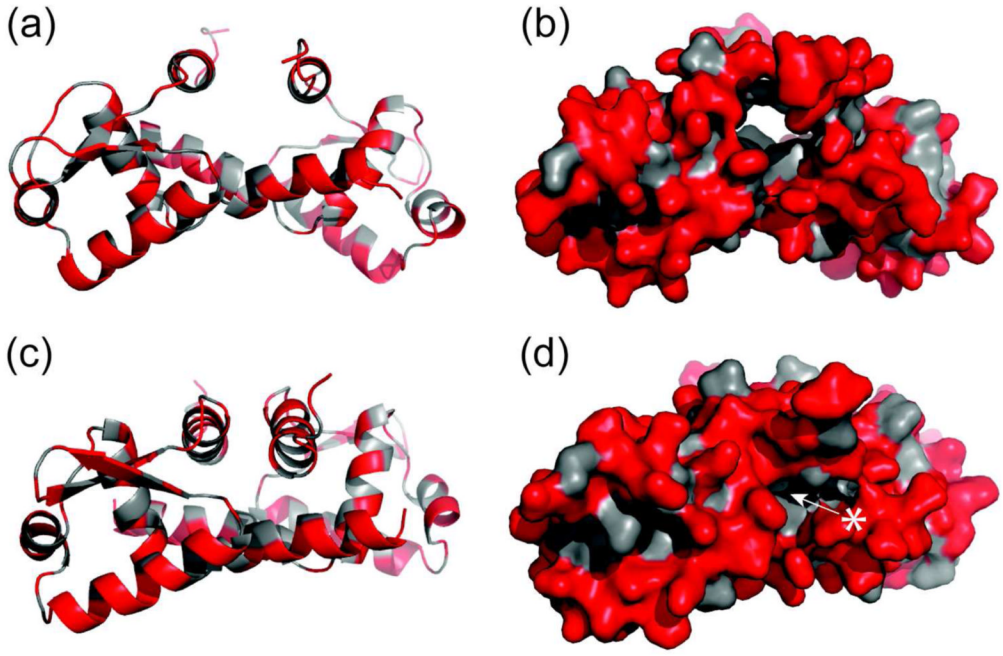

Figure 9.
Ribbon (a) and spacefill (b) diagrams of the solution structures of Zn(II)-CzrA (2KJC) and apo-CzrA bound to the CzrO DNA (2KJB)[15] (c) and (d). All apolar residues are shaded *gray* and polar residues are *red*. The Zn(II) chelate is not shown.[15] Note that these are identical views of these two conformations, looking down the dimer interface with respect to the C-terminal α5 helices. A solvent exposed pore dominated by hydrophobic residues, clearly visible in the DNA-bound state (b), significantly expands a small internal aqueous cavity in the Zn_2-CzrA conformation (d, the entrance of which is marked by the asterisk), and is derived from the hydrophobic core of the homodimer.

Table 1

Uncorrected thermodynamic parameters derived from direct analysis of isothermal titration calorimetry (ITC) experiments[a]

Buffer	T (°C)	n_1	K_1 (× 10^6 M^{-1})	ΔH_1 (kcal mol^{-1})	n_2	K_2 (× 10^6 M^{-1})	ΔH_2 (kcal mol^{-1})
Zn → apo-CzrA (3 mM NTA)							
HEPES	15	N/A	11.6 ± 0.5	−0.2 ± 0.3	N/A	0.93 ± 0.04	−4.8 ± 0.2
HEPES	25	N/A	75 ± 9	−3.00 ± .08	N/A	4.7 ± 0.6	−6.0 ± 0.3
HEPES	35	N/A	9 ± 1	−5.08 ± .07	N/A	0.7 ± 0.1	−7.4 ± 0.2
Bis-Tris	25	N/A	22 ± 11	−4.02 ± .07	N/A	1.1 ± 0.2	−6.98 ± 0.05
ACES	25	N/A	85 ± 50	−3.7 ± 0.2	N/A	4.3 ± 0.9	−6.8 ± 0.2
Mops	25	N/A	26 ± 7	−2.08 ± 0.09	N/A	1.4 ± 0.1	−5.9 ± 0.1
Zn → CzrA•CzrO (10 mM Imidazole)							
HEPES	25	0.8 ± 0.1	2000 ± 2000	−5.3 ± 0.3	1.2 ± 0.2	200 ± 300	−0.7 ± 0.1
Bis-Tris	25	0.8 ± 0.2	7000 ± 4000	−5.3 ± 0.1	1.2 ± 0.1	200 ± 100	0.40 ± 0.04
ACES	25	0.8 ± 0.2	5000 ± 3000	−7 ± 1	1.2 ± 0.2	100 ± 200	1.5 ± 0.8
Mops	25	0.8 ± 0.2	1000 ± 2000	−6.1 ± 0.5	1.2 ± 0.2	80 ± 90	−1.0 ± 0.2
CzrA → CzrO							
HEPES	25	N/A	200 ± 100	−7.4 ± 0.2	N/A	1.2 ± 0.8	−2.3 ± 0.1

[a]Solution conditions: 50 mM indicated buffer, 400 mM NaCl, pH 7.0 at the indicated temperature. The chemical model used to fit the data is indicated in the text and K_1 and K_2 are generic designations for the first and second steps of a two-site reaction model. These refer to individual K_i as shown in Table 2.

Table 2

Buffer-independent thermodynamic parameters for the indicated equilibria at pH 7.0, 25.0 °C[a]

T (°C)	K_1[b] (×10^{11} M^{-1})	ΔH_1 (kcal mol^{-1})	$-T\Delta S_1$ (kcal mol^{-1})	K_2[b] (×10^{11} M^{-1})	ΔH_2 (kcal mol^{-1})	$-T\Delta S_2$ (kcal mol^{-1})
			Zn → apo-CzrA			
	K_1	ΔH_1	$-T\Delta S_1$	K_2	ΔH_1	$-T\Delta S_2$
25.0	12 ± 2	0.06 ± 0.2	−16.6 ± 0.8	0.6 ± 0.1	−2.9 ± 0.2	−11.9 ± 0.7
			Zn → CzrA•CzrO			
	K_5	ΔH_5	$-T\Delta S_5$	K_6	ΔH_6	$-T\Delta S_6$
25.0	0.04 ± 0.02	2.9 ± 0.3	−16.1 ± 0.8	0.005 ± 0.003	3.6 ± 0.1	−15.5 ± 0.9
			CzrA → CzrO			
	K_3	ΔH_3	$-T\Delta S_3$	K_{3a}	ΔH_{3a}	$-T\Delta S_{3a}$
25.0	1.3 ± 0.9	−7.4 ± 0.2	−7.8 ± 0.4	0.0062 ± 0.0005	−2.3 ± 0.1	−2.3 ± 0.1

[a] Solution conditions: 50 mM Hepes, 0.4 M NaCl, pH 7.0, 25.0 °C.

[b] K_1 and K_2 refer to generic step-wise equilibrium constants for the reactions indicated and correspond to the actual K_i (see Figure 2), ΔH_i and $-T\Delta S_i$ shown. Uncertainties shown reflect a propagation of the standard errors from multiple titrations as well as ~30% relative error associated with the number of protons released (see Figure 4) which propagates through ΔH_i and $-T\Delta S_i$.

Table 3

Homotropic and heterotropic coupling energies determined by ITC

Coupling Energies (kcal mol^{-1})			
	$\Delta(\Delta G)^a$ (25.0 °C)	$\Delta(\Delta H)$	$\Delta(-T\Delta S)$
Homotropic[b]			
CzrA	1.8 ± 0.7	−2.9 ± 0.3	4.7 ± 0.9
CzrA•CzrO	1.3 ± 0.9	0.7 ± 0.3	0.6 ± 0.7
Heterotropic[c]			
	ΔG_c^1	ΔH_c^1	$-T\Delta S_c^1$
Zn_1	3.4 ± 0.6	2.9 ± 0.4	0.5 ± 1
	ΔG_c^2	ΔH_c^2	$-T\Delta S_c^2$
Zn_2	2.9 ± 0.2	6.5 ± 0.3	−3.6 ± 1
	ΔG_c^t	ΔH_c^t	$-T\Delta S_c^t$
Total	6.3 ± 0.7	9.4 ± 0.5	−3.1 ± 1

[a] $\Delta(\Delta G) = \Delta(\Delta H) + \Delta(-T\Delta S)$.

[b] The homotropic coupling energies reflect the negatively cooperative Zn^{2+} binding to either apo CzrA complex ($\Delta H_2 - \Delta H_1$; $-T\Delta S_2 - (-T\Delta S_1)$ from Table 2) or the CzrA•CzrO ($\Delta H_6 - \Delta H_5$; $-T\Delta S_6 - (-T\Delta S_5)$ from Table 2).

[c] Heterotropic coupling energies describe the effect of Zn^{2+} on CzrA binding to CzrO DNA as a result of filling one meal site on the dimer (Zn_1) (*yellow* box, Figure 2; eq 5–7), the second site on the dimer, relative to the first (Zn_2) (*green* box, Figure 2; eq 8–10) or the cumulative effect of filling on both metal sites relative the reference apo-CzrA homodimer state (Figure 2-b; eq 2–4).